# Ventricular Tachycardia (VT) Substrate Characteristics: Insights from Multimodality Structural and Functional Imaging of the VT Substrate Using Cardiac MRI Scar, $^{123}$I-Metaiodobenzylguanidine SPECT Innervation, and Bipolar Voltage

Hasan Imanli*[1,2], Kiddy L. Ume*[1,2], Jean Jeudy[1,3], Tamunoinemi Bob-Manuel[1,2], Mark F. Smith[1,3], Wengen Chen[1,3], Mohammed Abdulghani[1,2], Yousra Ghzally[1,2,4], Jagat Bandhu Mahat[2], Refael Itah[5], Alejandro Restrepo[1,2], Vincent Y. See[1,2], Stephen Shorofsky[1,2], Vasken Dilsizian[1,3], and Timm Dickfeld[1,2]

*[1]Maryland Arrhythmia and Cardiology Imaging Group (MACIG), Baltimore, Maryland; [2]Division of Cardiology, Department of Medicine, University of Maryland School of Medicine, Baltimore, Maryland; [3]Department of Diagnostic Radiology and Nuclear Medicine, University of Maryland School of Medicine, Baltimore, Maryland; [4]Assiut University, Arab Republic of Egypt; and [5]Biosense Webster, Haifa, Israel*

Postischemic adaptation results in characteristic myocardial structural and functional changes in the ventricular tachycardia (VT) substrate. The aim of this study was to compare myocardial structural and functional adaptations (late gadolinium enhancement/abnormal innervation) with detailed VT mapping data to identify regional heterogeneities in postischemic changes. **Methods:** Fifteen patients with ischemic cardiomyopathy and drug-refractory VT underwent late gadolinium enhancement cardiac MRI (CMR), $^{123}$I-metaiodobenzylguanidine SPECT, and high-resolution bipolar voltage mapping to assess fibrosis (>3 SDs), abnormal innervation (<50% tracer uptake), and low-voltage area (<1.5 mV), respectively. Three-dimensional reconstructed CMR/$^{123}$I-metaiodobenzylguanidine models were coregistered for further comparison. **Results:** Postischemic structural and functional adaptations in all 3 categories were similar in size (reported as median [quartile 1–quartile 3]: CMR scar, 46.1 cm$^2$ [33.1–86.9 cm$^2$]; abnormal innervation, 47.8 cm$^2$ [40.5–68.1 cm$^2$]; and low-voltage area, 29.5 cm$^2$ [24.5–102.6 cm$^2$]; $P > 0.05$). However, any single modality underestimated the total VT substrate area defined as abnormal in at least 1 of the 3 modalities (76.0 cm$^2$ [57.9–143.2 cm$^2$]; $P < 0.001$). Within the total VT substrate area, regions abnormal in all 3 modalities were most common (25.2%). However, significant parts of the VT substrate had undergone heterogeneous adaptation (abnormal in <3 modalities); the most common categories were "abnormal innervation only" (18.2%), "CMR scar plus abnormal innervation only" (14.9%), and "CMR scar only" (14.6%). All 14 VT channel/exit sites (0.88 ± 0.74 mV) were localized to myocardium demonstrating CMR scar and abnormal innervation. This specific tissue category accounted for 68.3% of the CMR scar and 31.2% of the total abnormal postischemic VT substrate area. **Conclusion:** Structural and functional imaging demonstrated regional heterogeneities in the postischemic VT substrate not appreciated by any single modality alone. The coexistence of abnormal innervation and CMR scar may identify a particularly "proarrhythmic" adaptation and may represent a potential novel target for VT ablation.

**Key Words:** multimodality imaging; cardiac imaging; cardiac innervation; ventricular tachycardia

**J Nucl Med 2019; 60:79–85**
DOI: 10.2967/jnumed.118.211698

Intraprocedural electroanatomic mapping (EAM) determined from catheter-based voltage measurements is the gold standard for electrophysiologic substrate identification in ischemic cardiomyopathy. However, EAM is time-intensive, cannot completely represent complex intramural, 3-dimensional (3D) scar structures, and can result in mapping inaccuracies because of both suboptimal catheter contact and limited spatial resolution (*1*). Therefore, structural imaging assessing anatomic changes (e.g., late gadolinium enhancement [LGE] cardiac MRI [CMR] or multidetector CT (*1–4*)) and functional imaging assessing changes in cellular function (e.g., metabolism/innervation using $^{18}$F-FDG PET (*5,6*) and $^{123}$I-metaiodobenzylguanidine [$^{123}$I-MIBG] SPECT (*7,8*)) have both been investigated for better characterization of the 3D ventricular tachycardia (VT) substrate.

Both structural imaging and functional imaging demonstrated a good to moderate correlation with the voltage-defined VT substrate. However, small to moderate degrees of mismatch between structural imaging (CMR/CT) or functional imaging ($^{18}$F-FDG PET/$^{123}$I-MIBG innervation) and EAM suggested that postischemic adaptation may be a more complex, heterogeneous process affecting structural and functional properties of the VT substrate to variable degrees (*1,3,7–10*). To our knowledge, a comparison of structural and functional imaging properties and determination of their correlation with EAM/VT substrate data have not yet been performed.

Therefore, the aims of this single-center feasibility study were to perform a comparison of structural imaging changes (CMR fibrosis) and functional imaging changes ($^{123}$I-MIBG innervation)

Received Mar. 19, 2018; revision accepted May 22, 2018.
For correspondence or reprints contact: Timm Dickfeld, Division of Cardiology, Department of Medicine, University of Maryland School of Medicine, 22 S. Greene St., Baltimore, MD 21201.
E-mail: tdickfel@som.umaryland.edu
*Contributed equally to this work,
Published online Jun. 29, 2018.

and to determine their correlation with bipolar mapping data with the goals of providing novel insights into the regional adaptation of the postischemic VT substrate and of identifying the imaging characteristics of VT channel/exit sites.

## MATERIALS AND METHODS

### Study Protocols and Patient Population

This study was designed as a single-center feasibility study of consecutive patients who had ischemic cardiomyopathy and were scheduled for radiofrequency ablation for drug-refractory VT. Study protocols were approved by the University of Maryland Institutional Review Board, and all patients signed a written informed consent form.

### LGE CMR Acquisition Protocol

Electrocardiography-gated inversion recovery images were obtained with a 1.5-T scanner (Magnetom Avanto; Siemens) during diastole 10–15 min after the intravenous injection of gadobenate dimeglumine (0.1 mg/kg). Short- and long-axis 2-dimensional inversion recovery sequences (slice thickness: 8 mm; no gap; inversion time: 250–350 ms; repetition time: 725–950 ms; echo time: 1–4 ms; flip angle: 25°) were obtained after optimal nulling to assess LGE. When possible, a novel inversion preparation pulse with a wide inversion bandwidth (2.4 kHz) was used to reduce metal artifacts.

### LGE CMR Image Processing

The LGE CMR images were exported in the Digital Imaging and Communications in Medicine (DICOM) file format and processed with a CARTOSEG MR Segmentation Module (Biosense Webster). Epicardial or endocardial borders of the left ventricle (LV) were outlined in all sequential short-axis slices (Figs. 1A and 1B). Areas with metal artifacts were manually traced and excluded from further analysis. The scar was defined as voxels with intensities of greater than 3 SDs in a histogram-based analysis using a remote area of normal myocardium (*11,12*). Segmentation results were confirmed by an expert radiologist interpreter with more than 15 y of experience.

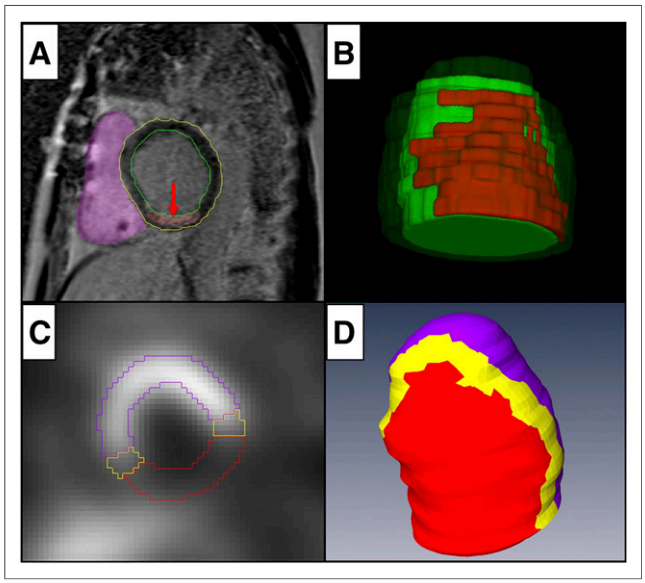


**FIGURE 1.** LGE CMR and $^{123}$I-MIBG SPECT reconstruction. (A) Epicardial (yellow line) and endocardial (green line) borders of LV outlined by manual segmentation of short-axis LGE CMR slices. RV (purple) reconstruction used to minimize rotational errors during registration. Scar reconstruction was based on voxel intensity (red arrow). (B) 3D reconstruction of myocardial scar (red) embedded in myocardial reconstruction (green). (C) $^{123}$I-MIBG SPECT short-axis slice demonstrating lack of uptake in inferolateral wall, consistent with abnormal innervation. (D) 3D reconstruction of $^{123}$I-MIBG SPECT innervation map with inferior view demonstrating normally innervated myocardium (purple), abnormally innervated myocardium (red; <50% uptake), and transition zone myocardium (yellow).

### $^{123}$I-MIBG Scintigraphy

Preprocedural $^{123}$I-MIBG SPECT images were obtained before VT ablation. Patients were administered 370 MBq (10 mCi) of $^{123}$I-MIBG (GE Healthcare) intravenously. SPECT imaging of the chest was performed using a dual-head γ-camera (SKYLight; Philips) 4 h after injection, with a minimum of 30 projections per head, 20–30 s/projection, and a 64 × 64 matrix. Camera heads were equipped with low-energy, high-resolution collimators, and all acquisitions were performed with a 20% energy window centered at the 159-keV photopeak of $^{123}$I.

### 3D $^{123}$I-MIBG Cardiac Map Reconstruction

3D reconstructions of myocardial innervation were created using Amira 5.4.2 software (Visage Imaging). On each 2-dimensional $^{123}$I-MIBG SPECT slice, areas of abnormally innervated myocardium (<50% tracer uptake) were determined visually by 2 masked, experienced cardiac nuclear medicine physicians with previously demonstrated intraobserver or interobserver variability of less than 10% (*8*). From the sequential 2-dimensional datasets, individual 3D innervation maps were created for each of the patients in the Amira environment (Figs. 1C and 1D). Right ventricle (RV) reconstruction was performed to correct for rotational errors during registration. The datasets were then converted to CARTO 3 System (Biosense Webster) readable mesh files using custom-made software (*7*).

### Voltage Map and VT Ablation

LV voltage maps were created through a retrograde/transseptal approach using a filling threshold of less than 10 mm and voltage settings of 0.5–1.5 mV. Bipolar signals were filtered at 10–400 Hz and were acquired during sinus rhythm or during ventricular pacing in patients with resynchronization therapy or pacemaker dependency. Any areas with a voltage of less than 1.5 mV were considered abnormal (*2,9,10,13*).

The ablation procedures were performed with a 3.5-mm open irrigated-tip catheter (THERMOCOOL or SF/SMARTTOUCH; Biosense Webster). The ablation target was any clinical VT documented by 12-lead electrocardiography or presumed clinical VT defined by matching cycle length, far-field morphology, and local electrogram–far-field electrogram relationship from implantable cardioverter–defibrillator recordings. First, sustained monomorphic VT matching the clinical or presumed clinical VT was induced to obtain a current 12-lead electrocardiography template. Second, pace map matches of greater than or equal to 11 or 12 leads with the longest stim-QRS interval were used to approximate the VT channel/exit site (*14,15*). Third, entrainment/activation mapping was performed to the maximum degree tolerated after reinduction of the VT to confirm the anatomic location of the VT channel/exit site, which was then used for further analyses (*14,15*). Radiofrequency ablation was performed orthogonally to the defined channel using single, overlapping radiofrequency lesions (40–50 W; 60 s each). After ablation, programmed electric stimulation with up to 3 extra stimuli and the shortest coupling interval (200 ms) from at least 2 RV/LV sites was repeated, and successful ablation was defined as the inability to induce the ablated clinical VT.

### 3-Way Comparison and Analysis

The 3D CMR and $^{123}$I-MIBG maps were transferred to the clinical CARTO 3 System using the CARTOMERGE Module (Biosense Webster). The maps were coregistered with high-density voltage maps by obtaining multiple matching landmark pairs (superior/inferior RV septal insertion, mitral valve, and apex and additional assessment of

ascending aorta) for a detailed 3-way analysis. Reconstructed areas were carefully traced jointly by 2 experienced operators on the EAM map because the current CARTO 3 System does not allow the simultaneous display of 2 different 3D reconstructions (Fig. 2). Area measurements were performed using the internal CARTO 3 System tools. Predefined abnormal tissue categories consisted of low-voltage areas (<1.5 mV [LowVolt]), scar defined by LGE CMR (>3 SDs [CMR-Sc]), and abnormally innervated myocardium (<50% tracer uptake [ABNINNERV]). This approach allowed additional myocardial stratification as single, double, and triple ischemic structural and functional adaptations (defined as abnormal in 1, 2, or all 3 modalities). Regions without complete information in all 3 modalities were excluded from the analysis.

### Statistical Analysis

SPSS (IBM) version 16.0 was used for statistical analyses. Continuous variables were expressed as medians and quartiles (quartile 1–quartile 3) or mean ± SD as appropriate. Comparisons between measurements were conducted with a nonparametric Mann–Whitney *U* test or *t* test. Differences were considered significant at a *P* level of <0.05.

## RESULTS

### EAM and VT Ablation for 15 Patients

Table 1 shows patient characteristics. Data are presented as mean ± SD or numbers and percentages (in parentheses) of patients who had ischemic cardiomyopathy and drug-refractory VT and who underwent VT ablation. Detailed EAM was available for all patients, with an average LV surface area of 249.5 $cm^2$ (217.5–327.6 $cm^2$), consisting of 653 ± 448 points. All EAM maps contained confluent areas of decreased voltage (<1.5 mV), consistent with the preexisting ischemic cardiomyopathy. One patient had no inducible VT. In the remaining 14 patients, 46 VT episodes were inducible, with 14 VT episodes representing the clinical or assumed clinical VT. Clinical VT episodes had a cycle length of 364 ms (339–424 ms) and originated from the interventricular septum ($n = 2$), from the inferior ($n = 7$), inferoseptal ($n = 1$), lateral ($n = 2$), or anterolateral ($n = 1$) wall, or from the apex ($n = 1$). After ablation, clinical VT episodes were no longer inducible by either complete ($n = 11$) or limited (because of hemodynamic instability; $n = 3$) programmed electric stimulation.

**TABLE 1**
Patient Characteristics

| Characteristic | No. | Percentage | Mean ± SD |
|---|---|---|---|
| Men | 13 | 87 | |
| Age at time of ablation (y) | | | 71.2 ± 7.7 |
| Ejection fraction (%) | | | 28 ± 10 |
| Presence of ICD at time of ablation | 13 | 87 | |
| Comorbidities | | | |
| Diabetes mellitus | 2 | 13 | |
| Hypertension | 10 | 67 | |
| Hyperlipidemia | 6 | 40 | |
| Atrial fibrillation | 4 | 27 | |
| Congestive heart failure | 6 | 40 | |
| Medications | | | |
| β-blocker | 15 | 100 | |
| ACEI/ARB | 13 | 87 | |
| Amiodarone | 9 | 60 | |
| Aldosterone antagonist | 1 | 7 | |
| Other antiarrhythmic drugs | 0 | 0 | |

ICD = implantable cardioverter defibrillator; ACEI = angiotensin-converting enzyme inhibitor; ARB = angiotensin receptor blocker.

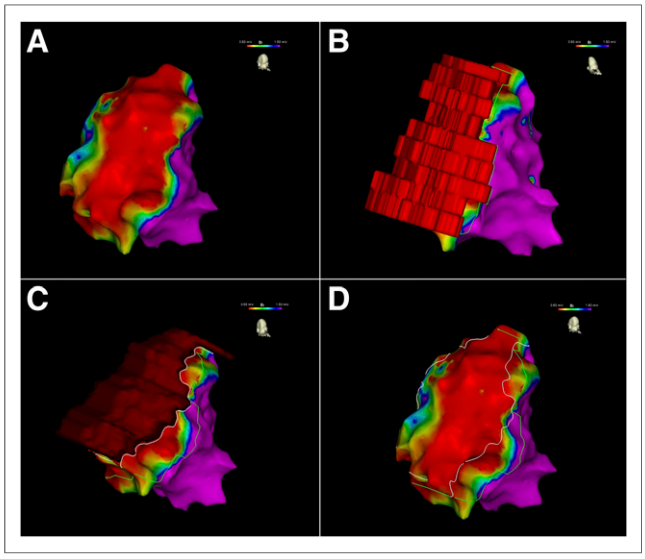


**FIGURE 2.** Comparison of 3D LGE CMR map, $^{123}$I-MIBG SPECT innervation map, and EAM map. (A) Bipolar EAM, inferior view, demonstrating inferior scar (red; <0.5 mV), border zone (yellow–blue; 0.5–1.5 mV), and normal voltage (purple; >1.5 mV). (B) Coregistration of EAM map and LGE CMR map. Green line demonstrates projected border of CMR-Sc. (C) Coregistration of EAM map and $^{123}$I-MIBG SPECT innervation map. White line demonstrates projected border of ABNINNERV zone. (D) EAM with green and white lines (B and C) corresponding to borders of abnormal myocardial areas. Mild rotational changes in B and C demonstrate perpendicular view used to accurately trace contours of CMR and innervation reconstruction.

### Triple-Modality Visualization

3D CMR scar maps were successfully reconstructed from sequential short-axis LGE images for all patients by use of the CARTOSEG MR Segmentation Module (reconstruction time, 10 ± 4 min). Thirteen of the 15 patients had in place an implantable cardioverter–defibrillator that caused a metal artifact affecting 12% ± 10% of the LV surface. Similarly, 3D innervation maps were generated for all patients on the basis of the short-axis $^{123}$I-MIBG SPECT innervation maps (*8*); the average reconstruction time was 23 ± 8 min. Two patients had noninterpretable areas on $^{123}$I-MIBG SPECT because of increased liver or lung uptake affecting 40% and 37% of the total LV area, respectively.

### Comparison of Abnormal Areas

Areas with a bipolar voltage of less than 1.5 mV (LowVolt), CMR scar (CMR-Sc), and abnormal innervation (ABNINNERV) were seen in all patients. The areas of LowVolt, CMR-Sc, and ABNINNERV were 29.5 $cm^2$ (24.5–102.6 $cm^2$), 46.1 $cm^2$ (33.1–86.9 $cm^2$), and 47.8 $cm^2$ (40.5–68.1 $cm^2$), respectively (Table 2); accounted for 23.3% (17.1%–42.0%), 35.1% (22.1%–49.5%), and

**TABLE 2**
Imaging Characteristics

| Characteristic | Area size ($cm^2$) | | Percentage of total VT substrate | |
|---|---|---|---|---|
| | Median | Quartile 1–quartile 3 | Median | Quartile 1–quartile 3 |
| CMR-Sc | 46.1 | 33.1–86.9 | 58.3 | 46.1–81.5 |
| ABNINNERV | 47.8 | 40.5–68.1 | 70.6 | 52.3–81.0 |
| LowVolt | 29.5 | 24.5–102.6 | 49.1 | 32.2–73.2 |
| Sum of all areas with 1 abnormality | 29.0 | 18.5–87.2 | 49.3 | 29.4–59.7 |
| Sum of all areas with 2 abnormalities | 25.7 | 12.6–34.0 | 23.3 | 19.3–33.1 |
| Area with 3 abnormalities | 15.1 | 9.9–38.2 | 21.0 | 12.4–38.7 |
| TotalVTSubstr | 76.0 | 57.9–143.2 | 100 | |

Data are continuous variables. Because results are expressed as medians, sum of areas with 1, 2, and 3 abnormalities is not exactly 100%.

36.6% (26.7%–45.0%) of the total analyzable LV area, respectively; and were similar in size (CMR-Sc vs. ABNINNERV, $P = 0.44$; ABNINNERV vs. LowVolt, $P = 0.09$; CMR-Sc vs. LowVolt, $P = 0.23$) (Fig. 3).

However, these areas of regional structural and functional adaptations were only partially colocalized. The total area of the VT substrate (TotalVTSubstr), defined as myocardium with any abnormal postischemic structural or functional adaptation in at least 1 of the 3 categories (LowVolt, CMR-Sc, or ABNINNERV), was 57.6% (52.2%–66.1%) of the total analyzable LV area. This category was significantly larger (Fig. 3) than any of the 3 single categories alone (TotalVTSubstr vs. CMR-Sc, $P < 0.0001$; TotalVTSubstr vs. ABNINNERV, $P < 0.0002$; TotalVTSubstr vs. LowVolt, $P < 0.0001$).

The areas of LowVolt, CMR-Sc, and ABNINNERV accounted for 49.1% (32.2%–73.2%), 58.3% (46.1%–81.5%), and 70.6% (52.3%–81.0%) of TotalVTSubstr, respectively.

The resulting regional heterogeneity of postischemic structural and functional adaptations within TotalVTSubstr is shown in Figure 4. The largest component, representing myocardium with abnormalities in all 3 categories, accounted for 25.2% of TotalVTSubstr.

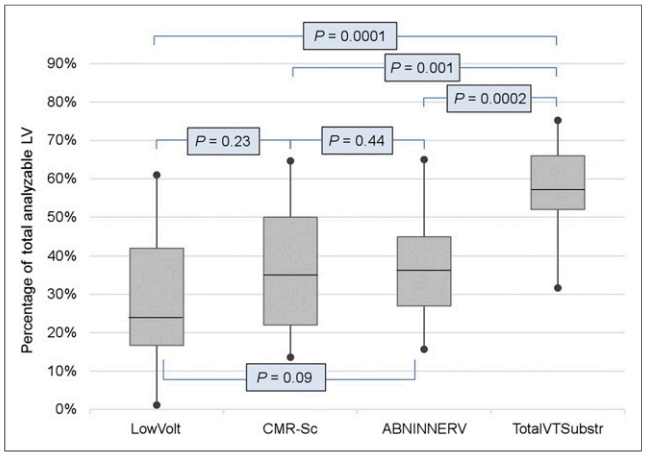


**FIGURE 3.** Graph showing percentages of LowVolt, CMRSc, ABNINNERV, and TotalVTSubstr out of total analyzable LV area.

However, significant components of TotalVTSubstr showed abnormalities in only 1 or 2 categories (Fig. 4). The largest of these areas had ABNINNERV only (18.2%), CMR-Sc and ABNINNERV (14.9%), and CMR-Sc only (14.6%).

The areas of myocardium with 1, 2, and 3 abnormalities accounted for 49.3% (29.4%–59.7%), 23.3% (19.3%–33.1%), and 21.0% (12.4%–38.7%) of TotalVTSubstr, respectively. The area with 1 abnormality was significantly larger than the area with 2 abnormalities ($P = 0.010$) or the area with 3 abnormalities ($P = 0.006$).

The CMR-Sc area overlapped the ABNINNERV and LowVolt areas in 68.3% (41.4%–83.1%) and 59.4% (33.0%–86.8%) of

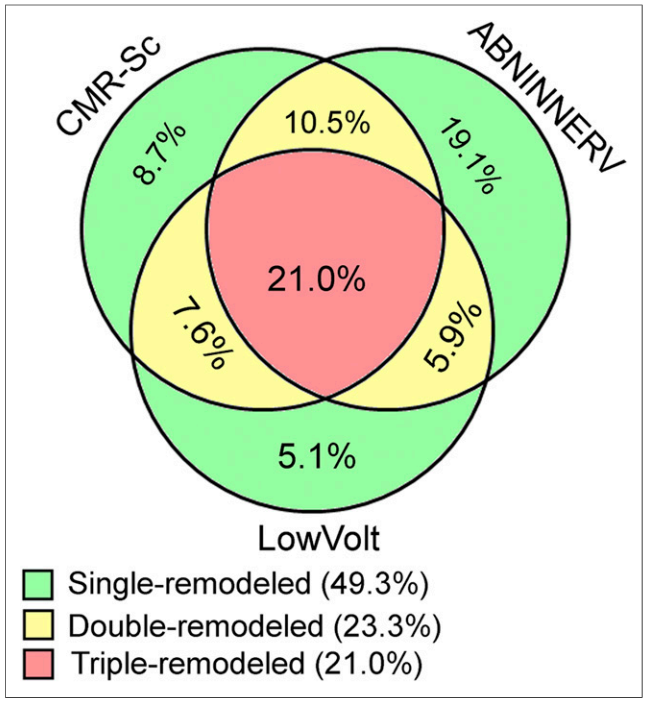


**FIGURE 4.** Comparison of abnormal areas (ABNINNERV, CMR-Sc, and LowVolt). Green indicates area with 1 abnormality, yellow indicates area with 2 abnormalities, and red indicates area with 3 abnormalities. Percentages are relative to TotalVTSubstr.

patients, respectively. The ABNINNERV area overlapped the CMR-Sc and LowVolt areas in 61.9% (38.2%–83.3%) and 52.3% (24.5%–69.9%) of patients, respectively. The LowVolt area overlapped the CMR-Sc and ABNINNERV areas in 68.3% (38.9%–83.3%) and 58.4% (47.0%–71.0%) of patients, respectively.

### Location of Ablation Sites

All VT channel/exit sites were located within TotalVTSubstr, demonstrating postischemic adaption, as shown in Figure 5. Additionally, none of the VT channel/exit sites were in areas that showed abnormalities in only 1 tissue category (CMR-Sc, ABNINNERV, or LowVolt); they were all localized in areas of 2 or 3 structural or functional adaptations.

Areas with abnormalities in all 3 categories—CMR-Sc, ABNINNERV, and LowVolt—harbored 12 of 14 successful ablation sites (86%) and accounted for 11.0% (6.1%–18.3%) of the total analyzable LV area, 21.0% (12.4%–38.7%) of TotalVTSubstr, and 42.8% (20.2%–66.0%) of the total CMR-Sc area (Fig. 5).

Importantly, all VT channel/exit sites were localized in areas with abnormalities in 2 categories—CMR-Sc and ABNINNERV. These areas accounted for 16.5% (15.5%–32.9%) of the total analyzable LV area, 31.2% (25.4%–57.2%) of TotalVTSubstr, and 68.3% (41.4%–83.1%) of the total CMR-Sc area.

Distances of the VT channel/exit sites from the closest borders of the CMR-Sc and ABNINNERV zones were 10.9 mm (3.2–15.3 mm) and 13.0 mm (3.4–18.9 mm), respectively.

## DISCUSSION

The present study demonstrated, for the first time (to our knowledge), that structural and functional imaging modalities can be combined to perform multimodality characterization of the postischemic VT substrate; that significant regional heterogeneities in structural and functional adaptations exist within the VT substrate; and that all VT channel/exit sites are within areas with ABNINNERV and CMR scar. These findings suggested a "proarrhythmic" structural and functional adaptation within the VT substrate.

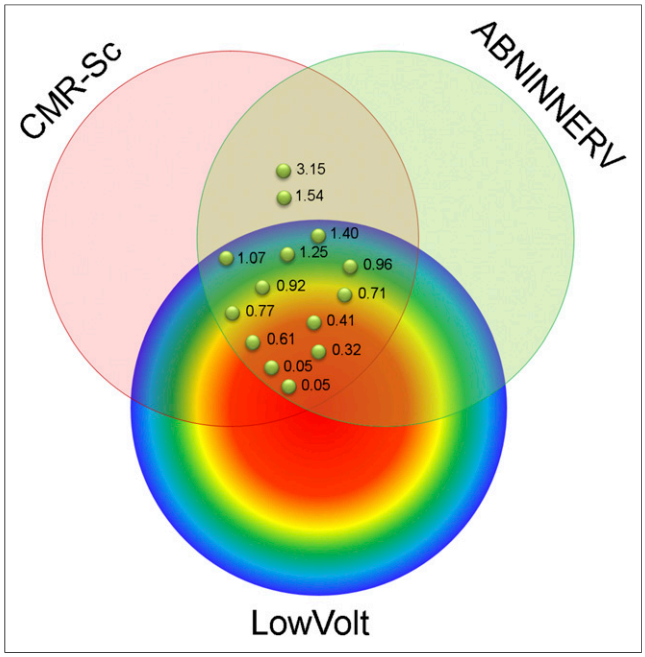


**FIGURE 5.** Successful VT channel/exit site location relative to CMR-Sc, LowVolt, and ABNINNERV. Different colors further stratify EAM of LowVolt area according to voltage. Each green point represents VT channel/exit site according to local bipolar voltage.

### Current VT Ablation Approaches

Because detailed entrainment/activation mapping without hemodynamic support is tolerated in only 10%–30% of cases (*16*), substrate-guided approaches targeting low-voltage areas in conjunction with fractionated signals, late/diastolic potentials, or local abnormal ventricular activity are frequently used (*17*). Unfortunately, long-term ablation success remains limited, with a sustained VT recurrence of 38% after 6 mo (*18*).

Structural imaging using either CT or CMR to identify LV scar by wall thinning or LGE has shown that successful ablation sites are usually located within those structurally abnormal areas (*1,4,10,19,20*). However, areas of structural changes are frequently large (>50 $cm^2$), and well-accepted imaging characteristics identifying proarrhythmic areas within the VT substrate have not been defined conclusively (*1,10,19*).

### Rationale for Combining Structural and Functional VT Substrate Assessments

Myocardial infarction results in tissue necrosis with significant structural and functional adaptations creating a complex proarrhythmic VT substrate. Various histologic adaptations (fibrofatty replacement; the presence of fibroblasts/dedifferentiated myofibroblasts) and functional adaptations (downregulation/lateralization of connexin 43; reductions in rapidly [$IK_r$] and slowly [$IK_s$] activating delayed rectifier potassium channels) have suggested a diverse process of post–myocardial infarction adaptation (*21*).

Structural imaging with LGE CMR accurately identifies areas of myocardial scar because of an accumulation of gadolinium in the increased interstitial space (*22*). 3D LGE CMR maps were reported to have the potential to assist in VT ablation procedures (*1,3,10,19*). However, histologically, fibrosis patterns ranged from homogeneous to patchy and to diffuse, with decreasing accuracy of detection by CMR. Prior studies of ischemic VT in which CMR scar was compared with EAM showed a good but imperfect correlation, with a significant mismatch in up to 1 of 3 patients (*3*), and a rather modest correlation with Cohen κ coefficients (ranging from 0.36 (*23*) to 0.7 (*24*)). Indeed, studies with CMR and EAM showed consistently high scar transmurality points with nearly preserved voltage (*1,3,10,19*), supporting the notion that bipolar amplitude and CMR-determined interstitial fibrosis are closely related but represent 2 nonidentical aspects of pathophysiologic scar remodeling.

The ability of functional imaging to assess various cellular adaptations after myocardial infarction represents another important but nonidentical aspect of scar remodeling. Autonomic innervation, a critical component of arrhythmogenesis, can be measured using the radiotracer $^{123}$I-MIBG (*6,7*). It can provide information about abnormal sympathetic innervation thought to mediate proarrhythmic risk via neurotransmitter accumulation. Indeed, the presence of abnormal cardiac autonomic innervation has been correlated with worsening heart failure outcomes (*25*), ventricular arrhythmia (*7,8,26,27*), and sudden cardiac arrest (*28*). Damaged myocardial presynaptic nerve terminals demonstrate reduced uptake of catecholamines by the uptake-1 mechanism (*29*), leading to the accumulation of neurotransmitters in the synaptic cleft, with downregulation of postsynaptic β-adrenergic receptors and an imbalance between

presynaptic signaling and postsynaptic signaling that favors proarrhythmia (*30*).

Swine and human studies demonstrated an increased sensitivity of myocardial nerve fibers to ischemia and colocalization of successful VT ablation sites with areas of abnormal innervation even in areas of preserved voltage (*7,29*).

### Structural and Functional Multimodality Imaging for Substrate Identification

The data suggest that structural as well as functional changes occur as adaptive mechanisms during postischemic remodeling. LGE CMR, myocardial innervation, and myocardial voltage (as another functional measure of myocardial cell integrity) all describe closely related but different aspects of the complex pathophysiologic VT substrate.

The present study demonstrated the presence of heterogeneous structural and functional adaptations of the VT substrate. The myocardial area affected by adaptation was larger than that predicted by any single modality. Significant areas with abnormalities in only 1 or 2 modalities existed in the postischemic scar substrate along with areas with abnormalities in 3 modalities, demonstrating a complex mixture of postischemic myocardial adaptions.

The fibrotic substrate has been proven to be a critical part of the VT substrate (*31,32*). However, recent high-density mapping studies demonstrated that a functional block is just as important as an anatomically fixed block (transmural fibrosis) in sustaining VT (*33*). These data imply that additional functional properties of the not fully scarred myocardium are important components of proarrhythmicity.

The present study suggested an interplay of structural and functional adaptations in arrhythmogenesis. Innervation was chosen for the present study because swine and human studies supported a direct role of innervation and colocalization with successful VT ablation sites (*7,26,29*). The finding of the present study that all VT channel/exit sites were located in abnormally innervated CMR scar suggested possible functional modulation of the anatomic VT substrate. The fact that all ablation sites were in areas with at least 2 abnormal categories raises the question of whether a certain threshold of adaptation is required to enable proarrhythmicity.

Combining structural and functional assessments may allow the identification of additional proarrhythmic areas that are more likely to enable VT circuits now and possibly VT recurrences later on. This method may allow more sophisticated assessments of the VT substrate and enable new pathophysiologic insights and novel approaches to imaging-guided VT ablation.

### Limitations

The present study represents a small, single-center, hypothesis-generating trial, and the findings need to be validated by additional and larger studies. Our findings are limited to patients with ischemic cardiomyopathy, and assessments with the nonischemic patient population are needed.

In the present study, the well-established n-SD method and a 50% $^{123}$I-MIBG cutoff derived from prior studies (*7,8*) were used to identify scar in CMR images. Analysis of alternative CMR scar identification algorithms or $^{123}$I-MIBG cutoffs should be included in future studies.

The $^{123}$I-MIBG SPECT data were acquired on a SPECT system without an integrated CT scanner, and images were reconstructed without attenuation correction. Abnormally innervated myocardium was assessed visually by 2 nuclear medicine physicians experienced in interpreting SPECT cardiac perfusion scans reconstructed without attenuation correction. Nonetheless, the results of the present study should be validated for SPECT/CT systems when attenuation correction is performed.

A careful review of data quality was performed to compensate for differences in spatial resolution (such as mapping density, CMR slice thickness, or SPECT camera technology). However, differences in spatial resolution are inherent in any multimodality imaging study. Similarly, registration errors are difficult to avoid in multimodality comparisons, but great care was taken during the modality registration to minimize any misregistration by using multiple reviews or reviewers and additional structures, such as the RV or aorta, to optimize coregistration.

## CONCLUSION

Combined structural and functional VT substrate characterization can demonstrate heterogeneities of regional structural and functional postischemic remodeling. The data provide novel insights into the myocardial adaptations affecting the ischemic VT substrate and its proarrhythmicity. The tissue category of abnormally innervated CMR scar may represent a functional and structural state that favors ventricular arrhythmia and may enable the identification of novel VT ablation targets.

## DISCLOSURE

Timm Dickfeld received consulting and grant support from Biosense Webster and grant support from GE Healthcare. Mark F. Smith and Vasken Dilsizian received grant support from GE Healthcare. Refael Itah is an employee of Biosense Webster. No other potential conflict of interest relevant to this article was reported.


## ACKNOWLEDGMENTS

We thank Frank M. Masters and Elizabeth S. Gault for their continued support and dedication to electrophysiology research to improve the lives of thousands of patients.


## REFERENCES


1. Dickfeld T, Tian J, Ahmad G, et al. MRI-guided ventricular tachycardia ablation: integration of late gadolinium-enhanced 3D scar in patients with implantable cardioverter-defibrillators. *Circ Arrhythm Electrophysiol.* 2011;4:172–184.
2. Tian J, Jeudy J, Smith MF, et al. Three-dimensional contrast-enhanced multidetector CT for anatomic, dynamic, and perfusion characterization of abnormal myocardium to guide ventricular tachycardia ablations. *Circ Arrhythm Electrophysiol.* 2010;3:496–504.
3. Codreanu A, Odille F, Aliot E, et al. Electroanatomic characterization of postinfarct scars: comparison with 3-dimensional myocardial scar reconstruction based on magnetic resonance imaging. *J Am Coll Cardiol.* 2008;52:839–842.
4. Yamashita S, Sacher F, Hooks DA, et al. Myocardial wall thinning predicts transmural substrate in patients with scar-related ventricular tachycardia. *Heart Rhythm.* 2017;14:155–163.
5. Dickfeld T, Lei P, Dilsizian V, et al. Integration of three-dimensional scar maps for ventricular tachycardia ablation with positron emission tomography-computed tomography. *JACC Cardiovasc Imaging.* 2008;1:73–82.
6. Duell J, Dilsizian V, Smith M, Chen W, Dickfeld T. Nuclear imaging guidance for ablation of ventricular arrhythmias. *Curr Cardiol Rep.* 2016;18:19.
7. Klein T, Abdulghani M, Smith M, et al. Three-dimensional $^{123}$I-meta-iodobenzylguanidine cardiac innervation maps to assess substrate and successful ablation sites for ventricular tachycardia: feasibility study for a novel paradigm of innervation imaging. *Circ Arrhythm Electrophysiol.* 2015;8:583–591.
8. Abdulghani M, Duell J, Smith M, et al. Global and regional myocardial innervation before and after ablation of drug-refractory ventricular tachycardia assessed with $^{123}$I-MIBG. *J Nucl Med.* 2015;56(suppl):52S–58S.

9. Tian J, Smith MF, Chinnadurai P, et al. Clinical application of PET/CT fusion imaging for three-dimensional myocardial scar and left ventricular anatomy during ventricular tachycardia ablation. *J Cardiovasc Electrophysiol.* 2009;20: 567–604.
10. Wijnmaalen AP, van der Geest RJ, van Huls van Taxis CF, et al. Head-to-head comparison of contrast-enhanced magnetic resonance imaging and electroanatomical voltage mapping to assess post-infarct scar characteristics in patients with ventricular tachycardias: real-time image integration and reversed registration. *Eur Heart J.* 2011;32:104–114.
11. Neilan TG, Coelho-Filho OR, Danik SB, et al. CMR quantification of myocardial scar provides additive prognostic information in nonischemic cardiomyopathy. *JACC Cardiovasc Imaging.* 2013;6:944–954.
12. Yan AT, Shayne AJ, Brown KA, et al. Characterization of the peri-infarct zone by contrast-enhanced cardiac magnetic resonance imaging is a powerful predictor of post-myocardial infarction mortality. *Circulation.* 2006;114:32–39.
13. Komatsu Y, Cochet H, Jadidi A, et al. Regional myocardial wall thinning at multidetector computed tomography correlates to arrhythmogenic substrate in postinfarction ventricular tachycardia: assessment of structural and electrical substrate. *Circ Arrhythm Electrophysiol.* 2013;6:342–350.
14. Bogun F, Good E, Reich S, et al. Isolated potentials during sinus rhythm and pace-mapping within scars as guides for ablation of post-infarction ventricular tachycardia. *J Am Coll Cardiol.* 2006;47:2013–2019.
15. Soejima K, Suzuki M, Maisel WH, et al. Catheter ablation in patients with multiple and unstable ventricular tachycardias after myocardial infarction: short ablation lines guided by reentry circuit isthmuses and sinus rhythm mapping. *Circulation.* 2001;104:664–669.
16. Stevenson WG, Wilber DJ, Natale A, et al. Irrigated radiofrequency catheter ablation guided by electroanatomic mapping for recurrent ventricular tachycardia after myocardial infarction: the Multicenter Thermocool Ventricular Tachycardia Ablation Trial. *Circulation.* 2008;118:2773–2782.
17. Pedersen CT, Kay GN, Kalman J, et al. EHRA/HRS/APHRS expert consensus on ventricular arrhythmias. *Heart Rhythm.* 2014;11:e166–e196.
18. Marchlinski FE, Haffajee CI, Beshai JF, et al. Long-term success of irrigated radiofrequency catheter ablation of sustained ventricular tachycardia: post-approval THERMOCOOL VT Trial. *J Am Coll Cardiol.* 2016;67:674–683.
19. Desjardins B, Crawford T, Good E, et al. Infarct architecture and characteristics on delayed enhanced magnetic resonance imaging and electroanatomic mapping in patients with postinfarction ventricular arrhythmia. *Heart Rhythm.* 2009;6: 644–651.
20. Tian J, Ahmad G, Mesubi O, Jeudy J, Dickfeld T. Three-dimensional delayed-enhanced cardiac MRI reconstructions to guide ventricular tachycardia ablations and assess ablation lesions. *Circ Arrhythm Electrophysiol.* 2012;5:e31–e35.
21. Arevalo H, Plank G, Helm P, Halperin H, Trayanova N. Tachycardia in post-infarction hearts: insights from 3D image-based ventricular models. *PLoS One.* 2013;8:e68872.
22. Kim RJ, Albert TS, Wible JH, et al. Performance of delayed-enhancement magnetic resonance imaging with gadoversetamide contrast for the detection and assessment of myocardial infarction: an international, multicenter, double-blinded, randomized trial. *Circulation.* 2008;117:629–637.
23. Tao Q, Piers SR, Lamb HJ, Zeppenfeld K, van der Geest RJ. Preprocedural magnetic resonance imaging for image-guided catheter ablation of scar-related ventricular tachycardia. *Int J Cardiovasc Imaging.* 2015;31:369–377.
24. Andreu D, Berruezo A, Ortiz-Pérez J, et al. Integration of 3D electroanatomic maps and magnetic resonance scar characterization into the navigation system to guide ventricular tachycardia ablation. *Circ Arrhythm Electrophysiol.* 2011;4: 674–683.
25. Jacobson AF, Senior R, Cerqueira MD, et al. Myocardial iodine-123 meta-iodobenzylguanidine imaging and cardiac events in heart failure: results of the prospective ADMIRE-HF (AdreView Myocardial Imaging for Risk Evaluation in Heart Failure) study. *J Am Coll Cardiol.* 2010;55:2212–2221.
26. Klein T, Dilsizian V, Cao Q, Chen W, Dickfeld TM. The potential role of iodine-123 metaiodobenzylguanidine imaging for identifying sustained ventricular tachycardia in patients with cardiomyopathy. *Curr Cardiol Rep.* 2013;15:359.
27. Boogers MJ, Borleffs CJ, Henneman MM, et al. Cardiac sympathetic denervation assessed with 123-iodine metaiodobenzylguanidine imaging predicts ventricular arrhythmias in implantable cardioverter-defibrillator patients. *J Am Coll Cardiol.* 2010;55:2769–2777.
28. Fallavollita JA, Heavey BM, Luisi AJ Jr, et al. Regional myocardial sympathetic denervation predicts the risk of sudden cardiac arrest in ischemic cardiomyopathy. *J Am Coll Cardiol.* 2014;63:141–149.
29. Sasano T, Abraham MR, Chang KC, et al. Abnormal sympathetic innervation of viable myocardium and the substrate of ventricular tachycardia after myocardial infarction. *J Am Coll Cardiol.* 2008;51:2266–2275.
30. Caldwell JH, Link JM, Levy WC, Poole JE, Stratton JR. Evidence for pre- to postsynaptic mismatch of the cardiac sympathetic nervous system in ischemic congestive heart failure. *J Nucl Med.* 2008;49:234–241.
31. de Bakker JM, van Capelle FJ, Janse MJ, et al. Slow conduction in the infarcted human heart: 'zigzag' course of activation. *Circulation.* 1993;88:915–926.
32. Stevenson WG, Khan H, Sager P, et al. Identification of reentry circuit sites during catheter mapping and radiofrequency ablation of ventricular tachycardia late after myocardial infarction. *Circulation.* 1993;88:1647–1670.
33. Tschabrunn CM, Roujol S, Nezafat R, et al. A swine model of infarct-related reentrant ventricular tachycardia: electroanatomic, magnetic resonance, and histopathological characterization. *Heart Rhythm.* 2016;13:262–273.